

MODELLING THE RADIO EMISSION FROM CYG OB2 #5: A QUADRUPLE SYSTEM?

M. KENNEDY

University of Victoria, Department of Physics and Astronomy, 3800 Finnerty Rd, Victoria, BC, Canada V8P 5C2

S.M. DOUGHERTY¹ AND A. FINK

National Research Council Herzberg Institute for Astrophysics Dominion Radio Astrophysical Observatory,
P.O. Box 248, Penticton, BC, Canada V2A 6J9

AND

P.M. WILLIAMS

Institute for Astronomy, Royal Observatory, Blackford Hill, Edinburgh, Scotland EH9 3HJ

Draft version July 6, 2021

ABSTRACT

Fifty observations at frequencies between 1.4 GHz and 43 GHz of the 6.6-day O6.5-7+O5.5-6 binary Cyg OB2 #5 using the Very Large Array over 20 years are re-examined. The aim is to determine the location and character of the previously detected variable radio emission. The radio emission from the system consists of a primary component that is associated with the binary, and a non-thermal source (NE), 0.8'' to the NE of the binary that has been ascribed to a wind-collision region (WCR) between the stellar winds of the binary and that of a B-type star (Star D) to the NE. Previous studies have not accounted for the potential contribution of NE to the total radio emission, most especially in observations where the primary and NE sources are not resolved as separate sources. NE shows no evidence of variation in 23 epochs where it is resolved separately from the primary radio component, demonstrating that the variable emission arises in the primary component. Since NE is non-variable, the radio flux from the primary can now be well determined for the first time, most especially in observations that do not resolve both the primary and NE components. The variable radio emission from the primary component has a period of 6.7 ± 0.3 years which is described by a simple model of a non-thermal source orbiting within the stellar wind envelope of the binary. Such a model implies the presence of a third, unresolved stellar companion (Star C) orbiting the 6.6-day binary with a period of 6.7 years and independent of Star D to the NE. The variable non-thermal emission arises from either a WCR between Star C and the binary system, or possibly from Star C directly. The model gives a mass-loss rate of $3.4 \times 10^{-5} M_{\odot} \text{ yr}^{-1}$ for Cyg OB2 #5, unusually high for an Of supergiant and comparable to that of WR stars, and consistent with an unusually strong He I 1.083- μm emission line, also redolent of WR stars. An examination of radial velocity observations available from the literature suggests reflex motion of the binary due to Star C, for which a mass of $23^{+22}_{-14} M_{\odot}$ is deduced. The natures of NE and Star D are also examined. If NE is a WCR, as suggested by other authors, then the required mass-loss rate is an order of magnitude higher than expected for an early B-type dwarf, and only just consistent with a supergiant. This raises the question of NE as a WCR, but its non-thermal luminosity is consistent with a WCR and a comparison of reddening between Cyg OB2 #5 and Star D do not rule out an association, implying Cyg OB2 #5 is a quadruple system. Pursuing alternative models for NE, such as an unassociated background source, would require very challenging observations.

Subject headings: stars:binaries – stars: early-type – stars:variables: other – radio continuum: stars – submillimetre

1. INTRODUCTION

Cyg OB2 #5 (V729 Cyg, BD +40 4220) is an eclipsing binary system consisting of two O-type supergiants orbiting in a 6.6-day period (Hall 1974; Leung & Schneider 1978; Rauw et al. 1999). This system is one of several luminous O-star systems in the Cyg OB2 association that shows evidence of variable radio emission (Persi et al. 1983, 1990; Bieging et al. 1989) in observations gathered over ~ 20 yrs. The radio emission appears to have two

states: a low-flux state of ~ 2 mJy at 4.8 GHz where the spectral index is consistent with thermal emission from a stellar wind, and a high-flux state of ~ 8 mJy at 4.8 GHz, where the spectral index is flatter than in the low state. The variations appear to have a ~ 7 -year period (Miralles et al. 1994) and have been attributed to variable non-thermal emission from an expanding plasmon arising in the binary (Bieging et al. 1989; Persi et al. 1990; Miralles et al. 1994).

Observations by Abbott et al. (1981) with the VLA revealed two radio components: a primary component associated with the binary and a secondary radio source (hereafter NE) $\sim 0.8''$ to the NE of the primary radio source. Miralles et al. (1994) confirmed the existence of

Electronic address: mgk@uvic.ca
Electronic address: sean.dougherty@nrc.ca, amy.fink@nrc.ca
Electronic address: pmw@roe.ac.uk
¹ University of Calgary, Department of Physics and Astronomy,
2500 University Dr. N.W., Calgary, AB, Canada T2N 1N4

NE and a 3 – 6 cm spectral index of -0.5 ± 0.3 hinted at non-thermal emission. Contreras et al. (1997) argue that this emission is the result of a wind-collision region (WCR) between the stellar wind of the binary and that of a B0-2 V star (hereafter Star D), $0.9''$ from the binary to the NE (Contreras et al. 1997).

All previous analyses of the radio emission from Cyg OB2 #5 are based on observations from the Very Large Array (VLA), obtained in all the different configurations of the array, and hence data covering different spatial frequency (i.e. baseline length) ranges. Dependent on the spatial frequency coverage, the observations may or may not resolve the emission from both the primary and NE components. None of the previous analyses in the literature have attempted to take this into account. Furthermore, no attempt has been made to determine either the continuum spectrum over a broad wavelength range or the location of the variable emission. As a result, not only is the nature of the radio emission from NE unknown, the evolution of the radio emission of the primary remains uncertain, which may account for the poor fits of models of the non-thermal emission to the observables (e.g. Miralles et al. 1994).

In this paper all VLA archive radio observations of Cyg OB2 #5 are re-examined to produce a consistently calibrated data set. The analysis accounts for the changes in the resolution of the array and presents a consistent treatment of the emission from both the primary and NE sources in each observation. For the first time, the nature of the emission of both the primary and NE can be determined throughout the ~ 20 years of the observations.

2. OBSERVATIONS

2.1. Very Large Array

A total of 50 VLA observations of Cyg OB2 #5 obtained between 1983 and 2003 were extracted from the NRAO archive. These data comprise 30 observations at 4.8 GHz (C band), 17 observations at 8.4 GHz (X band), 2 observations at 14.9 GHz (U band), and a single observation at 43.3 GHz (Q band). Examination of the few VLA observations at 1.4 GHz (L band) obtained in the low-resolution, C and D configurations were contaminated by extended low-surface brightness emission and were not incorporated in this study.

These data were edited and calibrated by a standard approach using the NRAO’s AIPS software package. Each observation was first examined to remove bad data. Phase-only antenna gain solutions were then established for all calibrators by self-calibration. Antennas showing random fluctuations in phase were examined closely, with further data editing as necessary. Both amplitude and phase calibration solutions were then derived for the calibrators. Again, further editing was applied as necessary. The absolute flux scale was established through bootstrapping the amplitude of the primary calibrator (either 3C286 or 3C84) to the phase calibrator, typically B2005+403 (\equiv J2004+404), giving a flux uncertainty typically determined to be $\sim 3 - 5\%$ ². Finally, phase and amplitude solutions of the phase calibrator were interpolated across the observations of Cyg OB2 #5. A final

TABLE 1
VLA OBSERVATIONS.

Date (Y/M/D)	MJD	Cfg.	Phase Calibrator Flux (Jy)	Primary Component Flux (mJy)	NE Component Flux (mJy)
1.4GHz					
87/10/16	47084	AB	5.17 ^{a,1}	2.98 \pm 0.13 ^b	
87/11/09	47108	AB	5.17 ¹	3.02 \pm 0.14	
4.8GHz					
83/08/18	45564	A	4.73	6.21 \pm 0.19	0.94 \pm 0.10
84/05/23	45843	C	4.23	8.15 \pm 0.24	
84/05/27	45847	C	3.02 ²	8.05 \pm 0.26	
84/09/06	45949	D	4.41	6.81 \pm 0.20	
84/09/15	45958	D	4.45	7.67 \pm 0.23	
84/09/20	45963	D	4.34	7.28 \pm 0.22	
84/09/22	45965	D	4.31	7.55 \pm 0.23	
84/09/24	45967	D	4.27	7.13 \pm 0.21	
84/09/28	45971	D	4.20	6.63 \pm 0.20	
84/10/16	45989	D	2.94 ²	8.41 \pm 0.25	
85/11/21	46309	D	4.04	5.37 \pm 0.16	
86/01/13	46443	D	4.14	4.18 \pm 0.13	
87/06/04	46952	D	3.56	3.75 \pm 0.16	
87/06/06	47196	D	3.60	3.90 \pm 0.27	
87/10/16	47084	AB	3.10 ¹	2.78 \pm 0.10	0.71 \pm 0.10
87/11/09	47108	AB	3.10 ¹	2.57 \pm 0.10	0.72 \pm 0.10
88/02/05	47196	B	3.10 ¹	4.15 \pm 0.22	
89/09/18	47787	BC	2.76	7.67 \pm 0.23	
92/11/02	48928	A	2.92	2.94 \pm 0.10	0.93 \pm 0.10
92/12/18	48974	A	3.01	2.70 \pm 0.10	0.74 \pm 0.10
92/12/19	48975	A	3.02	2.76 \pm 0.10	0.73 \pm 0.10
93/05/01	49108	B	3.06	2.56 \pm 0.10	0.85 \pm 0.10
93/12/27	49348	D	3.02	3.67 \pm 0.24	
94/04/09	49451	A	2.90	2.53 \pm 0.10	0.94 \pm 0.10
94/04/16	49458	A	2.90	2.37 \pm 0.10	0.84 \pm 0.10
95/04/27	49834	D	3.00	5.81 \pm 0.24	
95/06/10	49878	AD	3.15	5.13 \pm 0.15	0.89 \pm 0.10
95/06/12	49880	AD	3.14	5.16 \pm 0.15	0.64 \pm 0.10
97/01/04	50452	A	3.08	7.21 \pm 0.22	0.96 \pm 0.10
00/06/30	51725	CD	1.94 ³	3.30 \pm 0.10	
8.4GHz					
90/06/01	48043	AB	3.05	8.07 \pm 0.24	0.57 \pm 0.10
91/10/03	48532	AB	3.18	9.03 \pm 0.27	0.40 \pm 0.10
92/07/16	48819	D	3.18	6.99 \pm 0.21	
92/11/02	48928	A	3.15	4.27 \pm 0.13	0.66 \pm 0.10
92/12/19	48975	A	3.25	3.99 \pm 0.12	0.57 \pm 0.10
93/05/01	49108	B	3.23	4.11 \pm 0.12	0.39 \pm 0.10
93/10/31	49291	D	3.31	4.30 \pm 0.25	
93/12/27	49348	D	3.10	4.90 \pm 0.30	
94/04/09	49451	A	2.86	3.48 \pm 0.10	0.52 \pm 0.10
94/04/16	49458	A	2.90	3.39 \pm 0.10	0.65 \pm 0.10
95/04/27	49834	D	2.80	7.60 \pm 0.23	
96/02/02	50115	BC	2.88	7.84 \pm 0.24	
96/12/28	50445	A	2.91	8.08 \pm 0.24	0.62 \pm 0.10
98/07/17	51011	B	2.61	9.02 \pm 0.27	0.42 \pm 0.10
00/06/30	51725	CD	2.66 ³	3.82 \pm 0.16	
03/06/06	52796	A	3.01	7.17 \pm 0.22	0.36 \pm 0.10
03/09/09	52891	A	3.19	6.09 \pm 0.18	0.37 \pm 0.10
14.9GHz					
95/04/27	49834	D	9.49	9.39 \pm 0.47	
00/06/30	51725	CD	2.87 ³	5.27 \pm 0.26	
43.3GHz					
96/12/29	50446	A	1.13	12.17 \pm 0.61	

^a Name of the phase-reference calibrator used if not B2005+403 (\equiv J2004+404). 1=B2050+364; 2=B2200+420; 3=B2013+370.

^b Single values given for the flux are the total flux of emission from both the primary and secondary components.

² <http://www.vla.nrao.edu/astro/calib/manual/>

TABLE 2
MERLIN OBSERVATIONS

Date (Y/M/D)	MJD	Phase ^a Calibrator Flux (Jy)	Primary Component Flux (mJy)	Secondary Component Flux (mJy)
1.4GHz				
96/02/05	50118	3.18	4.57 ± 0.14	1.43 ± 0.14
96/03/14	50156	2.56	3.00 ± 0.16	1.33 ± 0.16
4.8GHz				
96/11/14	50401	3.02	5.82 ± 0.13	— ^b

^a Phase-reference calibrator was B2005+403 (\equiv J2004+404) for all observations.

^b NE was “resolved out”.

examination of the calibrated visibilities was made prior to image construction.

The visibility data for Cyg OB2 #5 were deconvolved via model fitting using the SMERF patch (Reid 2006) to the DIFMAP package (Shepherd et al. 1995). This is a technique used widely in VLBI image reconstruction, rather than the well-known CLEAN technique. An initial “best” model was established from imaging the 8.4-GHz visibilities obtained with the highest resolution, A configuration of the VLA. This was then used as the initial model for the remaining frequencies.

As noted previously, the radio emission from Cyg OB2 #5 consists of two components: the primary source associated with the O-star binary and NE, which is less bright than the primary. To establish models for both these sources, the model of the primary was first established. Phase-only self-calibration was then applied to further improve the antenna gain phase solutions derived initially from phase referencing alone. The model of NE was then established. The final model was determined by first fixing the location of NE and allowing the remaining model parameters to converge, before a final model fit with all parameters free to converge. Examples of the resulting deconvolved images at 8.4 GHz are shown in Fig. 1.

At 8.4 GHz, the two components were readily resolved in all observations obtained with A and B configuration of the VLA, whereas at 4.8 GHz the two components were only resolved in A-configuration observations. In all of these observations, NE was always detected. In C and D configurations, the two components are not resolved separately at any of the observing frequencies, with only a single unresolved source being observed.

The source fluxes were taken directly from the model-fitting parameters. The flux uncertainties at both 4.8 GHz and 8.4 GHz were taken to be the maximum of either the rms image uncertainty or 3% of the source flux. At both 14.9 GHz and 43.3 GHz, the uncertainty was taken to be the maximum of either the image rms or 5% of the flux. A summary of the observations and observed fluxes is presented in Table 1.

2.2. MERLIN

Three epochs of MERLIN observations were extracted from the MERLIN archive, with two observations (1996 February 5 and 1996 March 14) at 1.4 GHz (L band) and one observation (1996 November 14) at 4.8 GHz (C band). Editing and calibration of the visibilities was per-

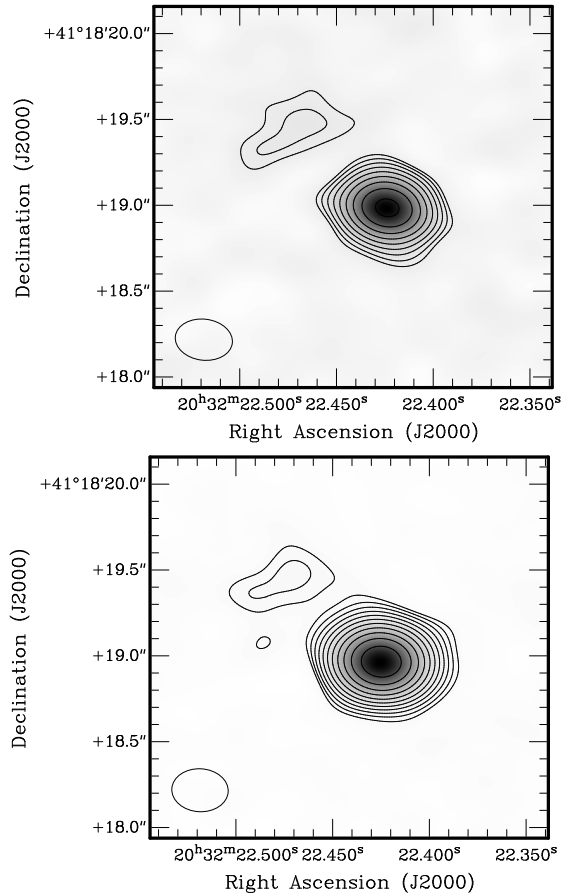


FIG. 1.— Two examples of the deconvolved VLA images at 8.4 GHz that show the primary and NE sources. The top image is from 1992 December 19 during a low emission state and the lower image is from 1996 December 28 during a high emission state. From these two images it is seen that the flux of the primary source increases between the low and high flux states, whereas the flux of NE remains constant. The position of the primary component is consistent with the position of the binary system. The first contour level is 3σ , where σ is the image rms, which is 0.044 mJy and 0.028 mJy in the top and bottom images respectively. The contour spacings represent increases by a factor of 1.5 from the 3σ level. The FWHM of the synthesized beam is shown in the lower left corner of the images.

formed using AIPS in a similar fashion to the VLA observations. The different performance of the individual telescopes of the MERLIN array was accounted for by applying different weights to each antenna according to their sensitivity³. As in the VLA observations, the observations were phase referenced using B2005+403 and the absolute flux scale was established from 3C286. The visibility data for Cyg OB2 #5 were deconvolved similarly to the VLA observations through modelling with SMERF. However, no phase-only self calibration was performed during the modelling process due to the small number of elements in the array.

At 1.4 and 4.8 GHz, both NE and primary emission components are resolved individually with MERLIN. However, NE was heavily resolved due to the lack of low spatial frequency (i.e. short spacing) coverage in

³ http://www.merlin.ac.uk/user_guide/OnlineMUG/

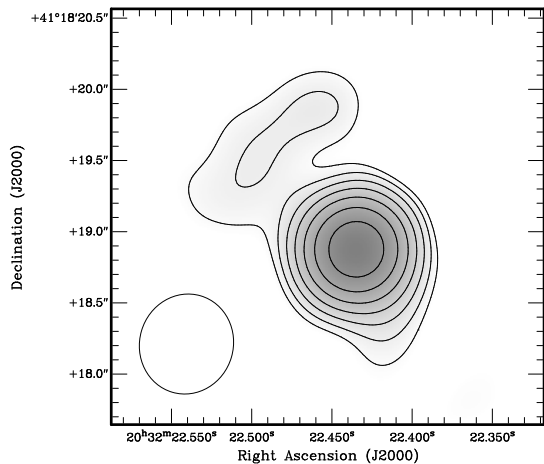


FIG. 2.— MERLIN image of Cyg OB2 #5 at 1.4 GHz from 1996 March 14, showing that both components are resolved. A taper of $250 \text{ k}\lambda$ was required to recover the secondary component. The resulting FWHM of the synthesized beam is shown in the lower left corner. The first contour level is 3σ , where σ is the image rms, which is 0.20 mJy . The contour spacings represent increases by a factor of 1.5 from the 3σ level.

the array. To address this issue, a Gaussian taper with HWHM of $250 \text{ k}\lambda$ was applied to the 1.4-GHz visibilities to increase the weight of the low spatial frequency data. At 4.8 GHz, NE was “resolved out” and only the primary component was detected. The primary emission model at 4.8-GHz had a major axis of 77 mas and an axial ratio of 0.90. A summary of the MERLIN observations is presented in Table 2. The flux uncertainties quoted are the rms image uncertainties. The deconvolved image from 1996 March 14 is shown in Fig. 2.

2.3. Submillimetre Observations

Two epochs of 350-GHz ($850 \mu\text{m}$) photometric observations of Cyg OB2 #5 were obtained during CANSERV time with the SCUBA bolometric receiver system on James Clerk Maxwell Telescope (JCMT). The first observation was taken on 1998 July 7 (MJD 51001) with the flux calibration established from the peak flux of the planetary map of Uranus. The second observation was taken on 1999 June 4 (MJD 51333) with Mars as the flux calibrator. Sky dipo were used at both epochs to determine the sky opacity. Data reduction and calibration were performed following a standard procedure using the SCUBA User Reduction Facility⁴. The observed fluxes at $850 \mu\text{m}$ were found to be $27 \pm 7 \text{ mJy}$ on 1998 July 7 and $47 \pm 8 \text{ mJy}$ on 1999 June 4. Given the sizes of the uncertainties in these values, their difference does not provide compelling evidence for variability. In the absence of additional submillimetre data to suggest otherwise, it is assumed that these radiometry data are consistent with each other.

2.4. Imaging and the NE Companion

An infrared K -band image of Cyg OB2 #5 was observed with the United Kingdom Infrared Telescope (UKIRT) on 1996 May 28 using the IRCAM3 camera

⁴ <http://docs.jach.hawaii.edu/star/sun216.htx/sun216.html>

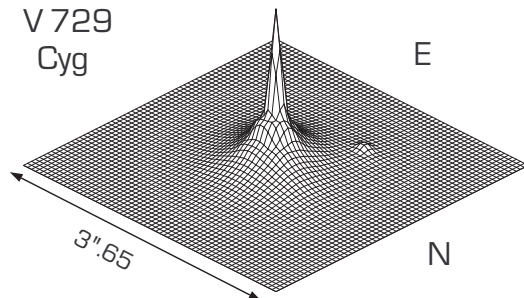


FIG. 3.— Maximum-entropy reconstruction of the $2.2\mu\text{m}$ image of V729Cyg oriented to show the companion to the NE (Star D) and drawn on a logarithmic intensity scale to compress the dynamic range.

and $5\times$ magnifier, giving an image scale of $0.057 \text{ arcsec pixel}^{-1}$. It was operated in shift-and-add mode, with each observation broken up into a large number of very short integrations. Provided that the field contains one, dominant point source (the central binary in this case), the centroid of this source on the array is located for each integration and the images are shifted in real time to bring them into alignment. Such a system is well suited to searching for faint companions to bright point sources and two such observations, each comprising 1000 integrations of 36-msec duration, were taken of Cyg OB2 #5. The same setup was used to observe HD 203856 at comparable airmass 30 minutes later to provide a point-spread function (PSF) calibrator. The reconstructed image is shown in Fig. 3.

Fig. 3 shows Star D to the NE, $0.90 \pm 0.03''$ from the central binary at a P.A. of $55 \pm 1^\circ$. This is consistent with the separations from the optical images ($0.98 \pm 0.06''$ at P.A. $61 \pm 7^\circ$ from CCD images and $0.948 \pm 0.043''$ at P.A. $54 \pm 4^\circ$ from Hipparcos) given by Contreras et al. (1997). The infrared magnitude difference between the binary and companion was measured to be $\Delta K = 3.1 \pm 0.1$. From photometric observations made with the Carlos Sánchez Telescope (Tenerife) in 1997, it is deduced that the system magnitude would have been $K = 4.52$ at the time of the imaging observation (phase 0.08 on the photometric elements of Linder et al. (2009)), giving $K = 7.6 \pm 0.1$ for Star D.

If Star D is associated with the central binary, it is expected to have the same reddening ($A_K = 0.7$, deduced from $A_V = 6.4$ Torres-Dodgen et al. 1991), and distance modulus (10.7, Torres-Dodgen et al. 1991) as Cyg OB2 #5, giving an absolute magnitude $M_K = -3.8$. This is ~ 0.5 magnitude too luminous for a B0 V star (cf. Vacca et al. (1996) with intrinsic $(V - K)$ from Ducati et al. (2001)), so it is suggested here that Star D is more evolved than a main sequence star, but probably not a giant. The luminosity class of Star D has been inferred previously from photometry, yet spectroscopy is necessary to determine both the stellar type and luminosity class.

3. ANALYSIS

3.1. Variations in Radio Emission

The fluxes of Cyg OB2 #5 at both 4.8 GHz and 8.4 GHz as a function of time are shown in Fig. 4. Through the 20 years of observations it is evident that

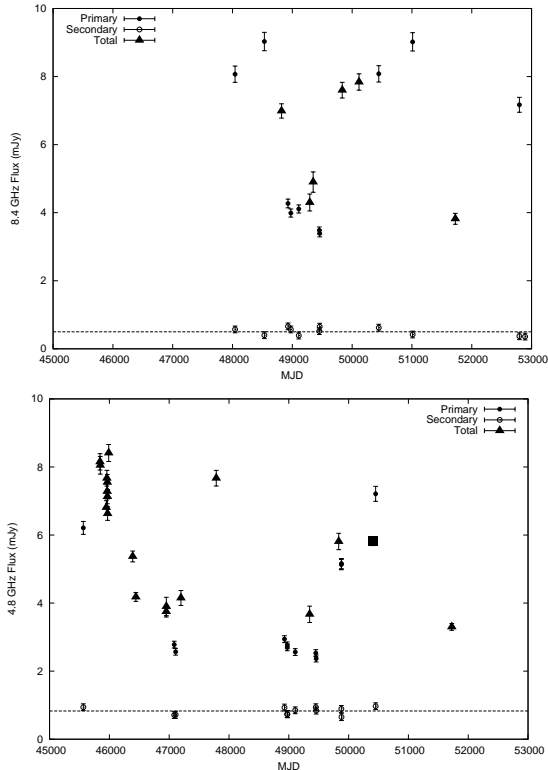


FIG. 4.— The fluxes of Cyg OB2 #5 between 1983 and 2003 at 8.4 GHz (top) and 4.8 GHz (bottom). Fluxes from the primary and NE are shown as solid and open symbols respectively. Those observations where the two components were *not* resolved as separate sources (i.e. primary+NE) are shown as triangles. The mean fluxes of NE at 4.8 GHz (0.83 ± 0.11 mJy) and 8.4 GHz (0.50 ± 0.12 mJy) are shown (dashed line). The MERLIN observation at 4.8 GHz is shown as a square.

the 4.8-GHz emission from Cyg OB2 #5 has cycled through three cycles of high and low emission with an approximate period of ~ 7 yrs, as first noted by Persi et al. (1985). It is also clear that the radio emission from NE shows no variation and the primary radio component is the source of the variations in Cyg OB2 #5.

At both 4.8 GHz and 8.4 GHz there were 12 and 11 epochs of VLA observations respectively where NE was resolved separately from the primary and a flux could be measured directly. These observations have a weighted-mean flux at 4.8 GHz of 0.83 ± 0.11 mJy and 0.50 ± 0.12 mJy at 8.4 GHz. The uncertainties are approximately equal to our minimum image uncertainty of 0.1 mJy and all the fluxes are within 1.7σ of these means. Hence, the 4.8 GHz and 8.4-GHz fluxes from NE are taken to be constant.

In some observations the primary and NE are not resolved separately and hence only a total flux for the system is determined. For these observations, the primary source flux was determined, for the first time, by subtracting the derived mean flux observed for NE from the total observed flux at each frequency.

Using fluxes from the primary at all observing epochs, the period of variation was determined using a string-length technique (Dworetzky 1983). This method was modified slightly to account for relative uncertainties in the flux values (van Loo et al. 2008). The period and its uncertainty were estimated from the string-length data as described by Fernie (1989). The string lengths as a

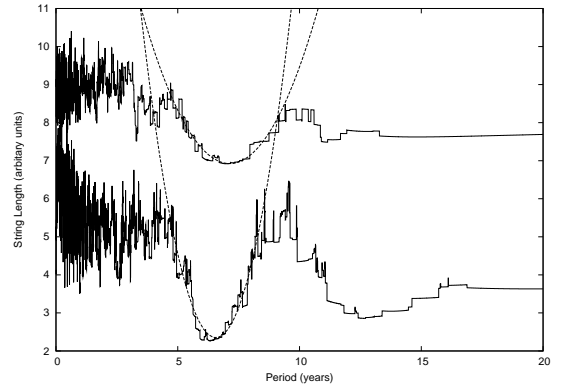


FIG. 5.— String lengths for 17 8.4-GHz observations (top) and 30 4.8-GHz observations (bottom). The derived period is 7.1 ± 0.5 years for the 8.4 GHz observations and 6.6 ± 0.3 years for the 4.8 GHz observations. Combined, these suggest a period of 6.7 ± 0.3 years.

function of period are presented in Fig. 5 for both the 4.8-GHz and 8.4-GHz observations, along with the best-fit parabolas from which the periods and associated uncertainties were derived. The derived periods of the variations are 6.6 ± 0.3 years at 4.8 GHz and 7.1 ± 0.5 years at 8.4 GHz. These are statistically consistent with each other and averaging these two results leads to an estimated emission variation period of 6.7 ± 0.3 years, which is remarkably similar to the “eyeball” period derived in previous works.

The string-length technique was also used to search for periodicity in the 4.8 GHz and 8.4 GHz observations consistent with the 6.6-day orbital period of the binary. In this case no clear minimum was discernible. This is not surprising as the sample rate of the observations is much lower than the Nyquist frequency of a 6.6-day period.

3.2. Spectral Indices of the Emission

The spectral index of a continuum spectrum is a characteristic of the underlying radio emission. Assuming the flux S_ν at frequency ν has a power-law behavior, $S_\nu \propto \nu^\alpha$, a weighted least-square fit is used to determine the spectral index α of each component in Cyg OB2 #5. MERLIN observations resolved the two radio components separately, giving a 1.4-GHz flux for NE. Since the two 1.4-GHz fluxes are the same within uncertainties, and only ~ 1 month apart, a mean flux of 1.38 ± 0.20 mJy was estimated for NE. In combination with the mean fluxes determined at 4.8 GHz and 8.4 GHz from the VLA observations, a spectral index of -0.50 ± 0.11 was derived for NE (Fig. 6). Higher frequency detections of NE would be useful to demonstrate if the power-law spectrum extends to higher frequencies.

Using both the VLA and MERLIN observations it was possible to determine the spectral index of the primary source at four different epochs of the flux variation cycle. Using only one MERLIN observation at 1.4 GHz and one VLA observation at 8.4 GHz from 1996 February during a high emission state, a spectral index of 0.26 ± 0.04 was calculated. Fluxes from the VLA at 4.8, 8.4 and 43.3 GHz during the same high flux state around 1996 December 29 give a spectral index of 0.24 ± 0.01 . In a fashion, the spectral index during two different low states was determined, with a spectral index of $0.51 \pm$

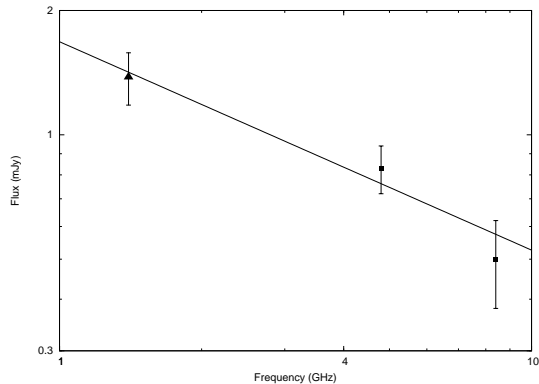


FIG. 6.— The spectrum of the secondary source NE, based on the fluxes of 1.38 ± 0.20 mJy, 0.83 ± 0.11 mJy, and 0.50 ± 0.12 mJy at 1.4, 4.8 and 8.4 GHz respectively. The 1.4 GHz observation (triangle) is from MERLIN and the 4.8 and 8.4 GHz data (squares) are from the VLA. The best-fit spectral index is -0.50 ± 0.12 .

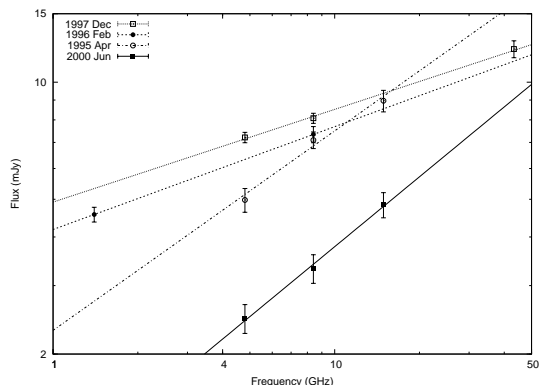


FIG. 7.— The change in the continuum spectra of the primary radio component between the low-flux state (solid squares) toward the high-flux state (open squares), passing through intermediate states (open and solid circles). The date of each set of observations is marked in the upper left corner. The best-fit power-laws are shown for each set of data, with values of 0.60 ± 0.04 (solid line), 0.51 ± 0.08 (dot-dashed line), 0.26 ± 0.04 (dashed) and 0.24 ± 0.01 (dotted). The continuum spectrum during the low-flux state has a spectral index consistent with thermal emission from a stellar wind, whereas during the high-flux state the spectrum is flatter. It is argued in Sec. 4.1 this is due to the addition of a non-thermal emission component to the thermal emission from the O-star binary.

0.08 on 1995 April 27 and 0.60 ± 0.04 on 2000 June 30 from the VLA. The 15-GHz fluxes for the primary were determined by subtracting an extrapolated 15-GHz flux for NE of 0.43 mJy that assumes the power-law spectrum for NE holds to 15 GHz. Examination of Fig. 6 suggests that a 15-GHz flux around 1 mJy would present a unique spectrum not observed previously in a WCR. Hence, it is estimated that the 15-GHz flux of NE, and hence the primary component, has a systematic error of less than ± 0.5 mJy, which still gives low-state continuum spectra consistent with thermal wind emission. These data and spectral indices are presented in Fig. 7. The two 350-GHz data points are consistent with the extrapolation of the radio data from the low-emission state and a thermal stellar-wind spectrum (Fig. 8).

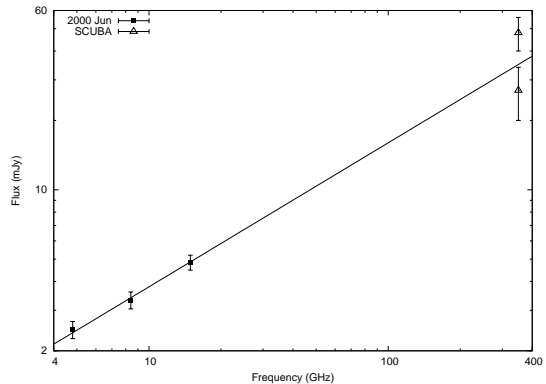


FIG. 8.— The radio fluxes from the primary component during a low-emission state shown with the 350-GHz JCMT data. The best-fit spectrum has a slope $+0.63 \pm 0.04$, consistent with a stellar wind. The JCMT data were not obtained during the radio minimum but fit this spectrum.

3.3. Proper Motion and Component Separation

A large number of observations spanning 20 years presents an opportunity to check for evidence of proper motion of the radio emission relative to the phase-reference source B2005+403. There is no evidence of proper motion in these data, with a scatter in positions of 100 mas, consistent with the positional uncertainty introduced by phase transfer at 4.8 GHz over $\sim 5^\circ$ between the phase calibrator and Cyg OB2 #5 using the VLA.

Absolute position uncertainties due to phase transfer do not impact determination of the relative position of the sources in the field. Using the models from seven epochs of 8.4-GHz observations obtained in the VLA A-configuration, the position of the NE relative to the primary was determined to be $+0.63 \pm 0.07''$ (East) and $+0.44 \pm 0.04''$ (North). This implies a component separation of $0.77 \pm 0.08''$ at a position angle of $55 \pm 2^\circ$ East of North, consistent with that derived from just two observation epochs by Contreras et al. (1997).

4. DISCUSSION

4.1. The Primary and Variable Emission

The primary emission component is associated with the O-star binary system and is the source of all the observed variations in the radio emission. In the low state the primary radio emission is found to have a spectral index of 0.60 ± 0.04 consistent with that expected for thermal emission arising in a steady-state radially symmetric stellar wind. The thermal emission must be reasonably constant in nature since the 350-GHz observations were not both obtained during a radio minimum yet are consistent with the stellar wind spectrum deduced from the radio minimum observations, with a best-fit spectral index 0.63 ± 0.04 across this broad frequency range (Fig. 8).

For a stellar wind, the mass-loss rate can be calculated from the radio flux (e.g. Wright & Barlow 1975). Assuming the stellar wind has a temperature of 10kK and a wind composition with ionic mean charge of 1, mean molecular mass of 1.5 and 1 electron/ion, and assuming all the thermal emission arises from the binary stellar wind (see below for discussion of another potential source of thermal emission), the 4.8-GHz flux at radio minimum

of 2.5 mJy leads to a deduced mass-loss rate of

$$\dot{M} = 3.4 \times 10^{-5} \times \left(\frac{v_\infty}{1500 \text{ km s}^{-1}} \right) \left(\frac{d}{1.7 \text{ kpc}} \right)^{3/2} \frac{1}{\sqrt{F}} M_\odot \text{ yr}^{-1},$$

where v_∞ is the terminal wind velocity, F is the volume filling factor (e.g. Abbott et al. 1981), and d is the distance to the source. The terminal velocity of 1500 km s^{-1} is adopted from Conti & Howarth (1999) based on the absorption component of the P-Cygni profile of the He I 1.083 μm line. It should be noted that the emission component of that line is very strong, and broader than those of other supergiants observed by them or in the atlas of Groh et al. (2007), more closely resembling line profiles in WN-type spectra.

The mass-loss rate derived here is consistent with other values determined for Cyg OB2 #5: $3.3 \times 10^{-5} M_\odot \text{ yr}^{-1}$ from UV lines (Howarth & Prinja 1989), $2.5 \times 10^{-5} M_\odot \text{ yr}^{-1}$ from infrared observations (Persi et al. 1990), $3.7 \pm 1.3 \times 10^{-5} M_\odot \text{ yr}^{-1}$ based on the 43-GHz flux (Contreras et al. 1996), adjusted for the terminal velocity of Conti & Howarth (1999) and for slight differences in adopted distance. More recently the reliability of these methods has been called into question as they tend to overestimate the actual mass-loss rate if the wind is clumpy (e.g. Mokiej et al. 2007; Fullerton et al. 2006). The most recent estimate of mass-loss rate in Cyg OB2 #5 is from Linder et al. (2009), who suggest a rate of $2.1 \pm 0.6 \times 10^{-5} M_\odot \text{ yr}^{-1}$ for the binary system based on the observed rate of period change. This is independent of distance and wind clumping but there are other processes which may affect the period. Nevertheless, all the mass-loss rate estimates are consistent with each other, though notably higher than values derived from model atmosphere fits for stars of similar spectral type (Mokiej et al. 2007), yet comparable to those of WR stars (Crowther 2007). This is consistent with the unusual strength of the He I 1.083- μm line in Cyg OB2 #5, indicating that the system, or one of its components, has a fast, heavy stellar wind comparable to those observed in WR stars.

As the flux increases from the low state toward the high state the continuum spectrum flattens out (see Fig. 7). This is consistent with the findings of Persi et al. (1990), who attributed the flattening to non-thermal emission from an expanding plasmon associated with the binary system. The model they produced resulted in broad agreement with the general variations in the data, though the fit to their data was poor.

Most recently, 3D-hydrodynamical models of O-star binary systems with periods of a few days have demonstrated that radio flux variations and the flatter spectral index can result from variable *thermal* emission arising in a WCR between the binary stars (Pittard 2009). Cyg OB2 #5 is a contact system (Leung & Schneider 1978) and the nature of a wind-collision region in such a system is unclear. However, such a region will emit thermal emission that is likely variable. Whether the flux and variation amplitudes can be attained in such a region is discussed further in Sec. 4.2,

An alternative model for the primary radio emission component is proposed here, where the lower spectral in-

dex during high emission is the result of the addition of a non-thermal component to the thermal emission from the binary system giving a ‘‘composite’’ spectrum. Such a model has been successfully applied to describe the relatively flat continuum spectra of some Wolf-Rayet stars (e.g. Chapman et al. 1999) where the non-thermal emission arises in a WCR between the wind of the WR star and that of a massive companion star.

For a system consisting of a non-thermal source embedded in a stellar wind plasma, the total observed flux is given as a function of frequency ν and at epoch t by

$$S_{obs}(\nu, t) = S_{th}(\nu) + S_{nt}(\nu, t) \quad \text{mJy.}$$

It is assumed the constant thermal emission component, $S_{th}(\nu)$, has spectral index of +0.6 and a flux at 4.8 GHz of 2.5 mJy, deduced from the the primary source during the low emission state. Hence

$$S_{th}(\nu) = 2.5 \left(\frac{\nu}{4.8} \right)^{0.6}.$$

The non-thermal emission component of the total flux, $S_{nt}(\nu, t)$, is modelled as

$$S_{nt}(\nu, t) = S_{4.8}(t) \left(\frac{\nu}{4.8} \right)^\alpha e^{-\tau(\nu, t)},$$

where $S_{4.8}(t)$ is the intrinsic 4.8-GHz flux of the non-thermal source at epoch t , α is the spectral index of the non-thermal emission assumed to be constant, and $\tau(\nu, t)$ is the line-of-sight free-free opacity through the stellar wind to the non-thermal source at frequency ν and epoch t , approximated by

$$\tau(\nu, t) \approx \tau_{4.8}(t) \left(\frac{\nu}{4.8} \right)^{-2.1}$$

where $\tau_{4.8}(t)$ is the 4.8-GHz line-of-sight free-free opacity at epoch t .

The line-of-sight opacity is dependent on the geometry of the line-of-sight to the non-thermal emission. Here, the case of a non-thermal source in orbit about the binary is considered. Williams et al. (1990) derived the varying free-free opacity along a line-of-sight to a non-thermal source orbiting in the circumbinary wind of the massive WR+O binary WR 140. Following Eqns. 12 and 14 in Williams et al. (1990), the opacity is dependent on the orbit inclination (i), argument of periastron (ω), as well as the epoch-dependent true anomaly (f) and the separation of the orbiting source from the companion star (r) in units of semi-major axis distance (a) such that

$$\tau_{4.8}(t) = \frac{\xi \sec i}{2\Delta r^3 \cos^3(\omega + f)} \times \left(\sin(\omega + f) \cos(\omega + f) \tan i + (1 + \tan^2 i) \arctan \left(\frac{-\sqrt{\Delta}}{\tan(\omega + f) \tan i} \right) \right), \quad (1)$$

where

$$\Delta = 1 + \tan^2(\omega + f) + \tan^2(i)$$

and ξ is a constant proportional to the square of the ion density in the stellar wind at a radius equal to the semi-major axis a , and related to C_{ff} in Williams et al. (1990)

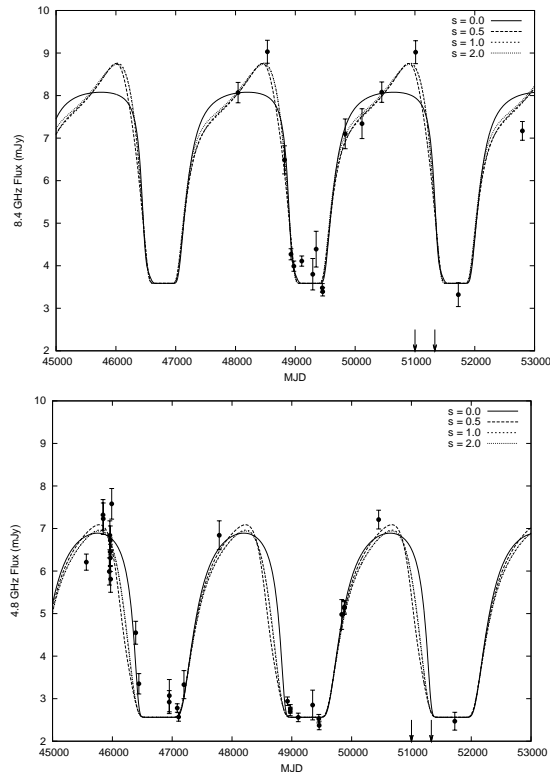


FIG. 9.— The best-fit orbiting non-thermal source model is shown against the observed fluxes of the primary at 8.4 GHz (top) and 4.8 GHz (bottom) for the $s = 0, 0.5, 1,$ and 2 models.

by

$$C_{\text{ff}} = \xi \left(\frac{\nu}{4.8} \right)^{-2.1}.$$

The intrinsic non-thermal flux $S_{4.8}(t)$ is expected to depend on the local conditions e.g. electron density, which will vary as the source moves through the dense circumbinary wind. This may be approximated by assuming a simple power-law relation with separation, namely

$$S_{4.8}(t) = S'_{4.8} r^{-s},$$

where $S'_{4.8}$ is the non-thermal flux when the separation is equal to a , and s is the power-law index. These definitions, along with the analytic solution to equation 1 (cf. Williams et al. 1990), allow $S_{\text{obs}}(\nu, t)$ to be determined as a function of the orbital phase of the non-thermal source orbiting the binary system.

A standard Levenberg-Marquart χ^2 -minimization technique was applied to both the 4.8-GHz and 8.4-GHz fluxes of the primary component to determine values for the seven free parameters in the model for each of the cases $s = 0, 0.5, 1,$ and 2 , assuming an orbital period of 6.7 years. Dougherty et al. (2003) suggest $s = 0.5$ for the non-thermal luminosity of a WCR. The resulting model parameters are given in Table 3 and the light curves arising from these models are plotted in Fig. 9. Fig. 10 shows the models for the $s = 0$ and $s = 0.5$ cases folded into the 6.7-year period.

Each of these simple models show a good fit to the data and are effective in matching observations at both frequencies across all four observed emission cycles through the 20 years of observation. The reduced- χ^2 values range

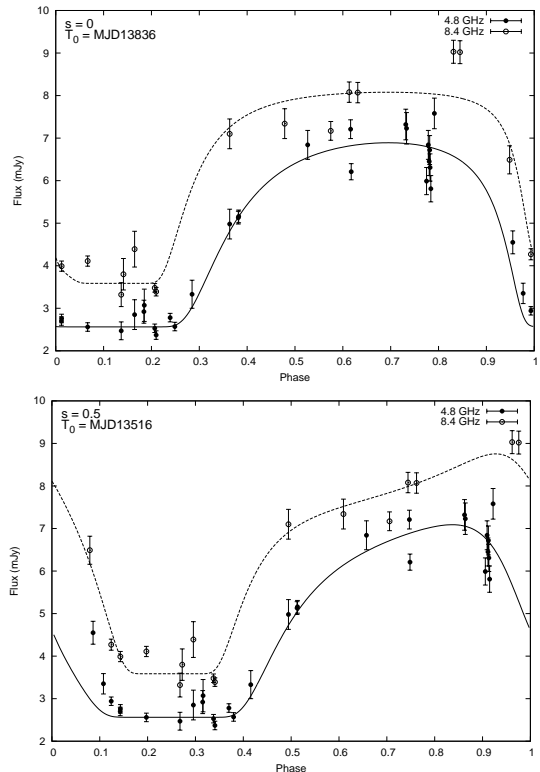


FIG. 10.— The best-fit orbiting non-thermal source model is shown for the $s = 0$ (top) and $s = 0.5$ (bottom) cases at 4.8 GHz (solid line) and 8.4 GHz (dashed line) against the fluxes of the primary, phased with a period of 6.7-year. Parameters for each model are given in Table 3.

from 4.4 to 4.6 indicating that each model has its flaws, with the $s = 0$ case being formally the best-fit. The $s = 0$ case corresponds to intrinsic non-thermal emission that is constant throughout the orbit i.e. the variation is caused entirely by the varying line-of-sight opacity. In this case the best-fit model is a good fit to the observations except it is too low to match the peak emissions at 8.4 GHz. Introduction of non-zero values for s gives models able to match these sharp emission peaks but the resulting model flux is too low to match the 4.8 GHz observations when the primary flux is in decline at MJD 46309 and MJD 46443 from the high to low emission state, just prior to radio minimum (around deduced orbital phase ~ 0.1).

Williams et al. (1990) could not fit the radio flux variations in WR 140 with this model and a single value of C_{ff} (corresponding to our ξ). This was attributed to the very different densities of the WR and O-star winds traversed by the line-of-sight at different orbital phases. The quality of the fits to the Cyg OB2 #5 radio-flux variations with a single value of ξ suggests that the stellar winds in this system have comparable densities, consistent with stars having comparable mass-loss rates rather than the ~ 30 -fold ratio between the WR and O-star winds in WR 140.

In all four models the stellar wind is completely opaque during the low emission state. Unfortunately the radio observation at both frequencies are not evenly distributed across the 20 years of observations and there are large gaps in the phase coverage of the observed light curves. Consequently the model fitting is unevenly fo-

TABLE 3
BEST MODEL-FIT PARAMETERS FOR THE ORBITING NON-THERMAL SOURCE MODEL.

s	$S'_{4.8}$ (mJy a^s)	α	ω ($^\circ$)	i ($^\circ$)	e	T_0 (MJD)	ξ
0	5.3 ± 0.5	-0.18 ± 0.25	319 ± 3	90 ± 40	0.69 ± 0.04	53836 ± 35	0.48 ± 0.13
0.5	6.4 ± 0.6	-0.34 ± 0.26	315 ± 3	90 ± 25	0.44 ± 0.04	53516 ± 34	0.62 ± 0.12
1	7.1 ± 0.6	-0.42 ± 0.28	352 ± 5	88 ± 46	0.23 ± 0.04	53636 ± 30	1.36 ± 0.22
2	7.6 ± 0.7	-0.47 ± 0.30	23 ± 5	85 ± 48	0.11 ± 0.05	53737 ± 31	1.64 ± 0.25

cused by the group of observations obtained during the low emission states. Based on the $s = 0$ model, the last low emission state occurred around 2007 February, and the next high emission state will occur around 2010 November.

The inclination across all models is consistent with an eclipsing orbit, though this parameter is poorly constrained. Likewise, even though the non-thermal spectral index tends to become more negative with increasing s , it is also poorly constrained. The non-thermal flux $S'_{4.8}$ increases with increasing s as would be expected: a greater flux fall-off with separation would require stronger emission to match the observations. Varying s ranges the time of periastron passage (T_0) by up to a year between the $s = 0$ and $s = 0.5$ cases, as evident in Fig. 10. The remaining T_0 values fall within this range. By far the greatest impact of varying the s parameter is on the deduced orbit eccentricity. For $s = 0$, the orbit eccentricity is high with $e \sim 0.7$, and as s increases the eccentricity decreases sharply, with $e \sim 0.1$ for the $s = 2$ case. As noted above, many of the observations were made during the low-state when the stellar-wind is opaque and the non-thermal emission does not contribute to the observed flux being fit by the model. This contributes to the uncertainties in the fitted parameters.

4.2. Evidence for a Third Star?

A non-thermal source orbiting the binary system requires a star (hereafter Star C) to be in a 6.7-year orbit around the binary. This star could contribute the non-thermal radio emission via a WCR arising from the collision of its own stellar wind with the wind from the O+O star binary (e.g. Eichler & Usov 1993). Such WCRs have been observed directly in some WR+O star and O+O star binary systems (e.g. Dougherty & Pittard 2006, and references therein). Alternatively, the non-thermal emission may arise from the putative third star directly, e.g. a compact object.

Given the high luminosities of the two supergiants in the binary and emission from circumstellar material, it will be very hard to detect the proposed third star directly, let alone measure its orbit. Instead, the radial velocities (RVs) of the central binary are examined to search for reflex motion due to it being in an orbit with Star C, as suggested by the radio observations.

The RVs measured by Rauw et al. (1999) come from four observing runs, each between 1 and 4 weeks duration and separated by about a year. As the variations should coincide with a period near 6.7 years, each of these runs is treated as a single observation. A fifth observation comes from the first five RVs measured by Bohannan & Conti (1976) in the space of a month 23 years earlier. For each

TABLE 4
MEAN RV DEVIATIONS (O-C) FROM THE O+O ORBIT AS A FUNCTION OF RADIO PHASE FOR FIVE OBSERVING RUNS.

MJD	ϕ	n (RVs)	mean (O-C)	σ
41150	0.81	5	14.9	9.0
49567	0.26	11	-7.6	6.7
49914	0.40	7	-2.2	6.6
50316	0.56	3	-3.7	7.3
50640	0.69	4	8.6	8.7

RV observed from the primary⁵, the residual (O-C) was calculated from the orbit by Rauw et al. (1999) (based on all the RVs) and formed the average (O-C) for each run. These are given in Table 4, together with the radio orbital phases calculated using $P = 6.7$ years and T_0 for the $s = 0$ model from Table 3.

A systematic increase of RV between phases 0.26 and 0.89 is seen, implying that the O+O binary moves away from us more rapidly. This implies that Star C moves towards us more rapidly in this phase interval so that the circumbinary extinction to the non-thermal radio source diminishes, consistent with it brightening during this orbital phase.

The run of mean (O-C) with phase is compared with the reflex motion of the O+O binary in orbit with Star C following the orbital elements of the embedded non-thermal radio source from the $s = 0$ case (see Fig. 11). Fitting

$$v_r = \gamma + K_{O+O}(e \cos \omega + \cos(f + \omega))$$

for K_{O+O} and systemic velocity γ , gives $K_{O+O} = 32 \pm 17 \text{ km s}^{-1}$ and $\gamma = -5.9 \pm 4.7 \text{ km s}^{-1}$, both very uncertain given the uncertainties in the (O-C)s and the shape of the RV curve in the phase range of the observations. The non-zero γ is a consequence of not weighting the mean (O-C)s by the rather unequal numbers of observations from which they were deduced. The mass function $f(m)$ can be derived from P (in days) and K (in km s^{-1}) from

$$\begin{aligned} f(m) &= \frac{m_C^3 \sin^3(i)}{(m_{O+O} + m_C)^2} \\ &= 1.036 \times 10^{-7} (1 - e^2)^{3/2} K^3 P, \end{aligned}$$

allowing an estimate of the mass, m_C , of Star C. From the data here, $f(m) = 3.2_{-2.8}^{+8.2} M_\odot$. Assuming $\sin(i) = 1$ and adopting $m_{O+O} = 41.5 \pm 3.4 M_\odot$ from Linder et al. (2009), this gives $m_C = 23_{-14}^{+22} M_\odot$ for Star C. The large

⁵ The secondary has not been used as Rauw et al. (1999) find a significantly lower γ -velocity for it in their orbit solution and attribute this to formation of the absorption lines in the wind

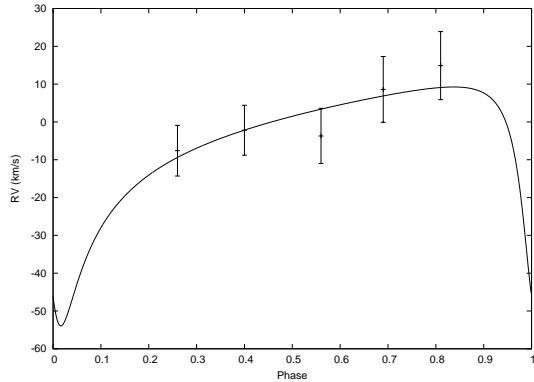


FIG. 11.— Comparison of observed (O–C) residuals, plotted with $2\text{-}\sigma$ error bars against radio phase, and the RV curve for the reflex motion corresponding to the elements of the $s = 0$ model (i.e. with ω shifted by 180° to reflect the location of the binary system in the orbit, rather than the 3rd star), with $K = 32 \pm 17 \text{ km s}^{-1}$ and $\gamma = -5.9 \pm 4.7 \text{ km s}^{-1}$ giving the best-fit of the observables.

uncertainty in the mass stems from the high relative uncertainty in K and the K^3 -dependence of $f(m)$.

With a paucity of observations, most especially at phases of the putative orbit where the radial velocity changes most dramatically, the uncertainties in this analysis are high. However, until further observations can be obtained to test this analysis, it remains a tantalizing piece of evidence that Cyg OB2 #5 is a tertiary system rather than a binary.

Additional support for Star C comes from X-ray data that reveal a hard component. Linder et al. (2009) suggest this is likely to arise in a WCR and argue that in such a compact binary like Cyg OB2 #5 the stellar winds of each component are far from achieving terminal velocity and the resulting X-ray emission would be rather soft. Hence they suggest a WCR would be between the binary and another star. Such a WCR between the binary and Star C provides a ready source for the non-thermal radio emission in the model described in Sec. 4.1. Such a mechanism has been widely established for WR stars and many O star systems that exhibit non-thermal emission (De Becker 2007). A mass of $\sim 23 M_\odot$ for Star C is consistent with a late O/early B-type star, which would have a sufficiently strong stellar wind to produce a WCR with the binary system wind in an orbit of size $\sim 14 \text{ AU}$.

The recent models of thermal emission in WCRs by Pittard (2009) raise the possibility that variable plasma density in a WCR between the binary and star C might account for the variable radio emission. Given the separation of the 6.7-year orbit, a WCR between the binary and Star C is undoubtedly adiabatic (certainly away from orbit periastron) and thus any thermal free-free emission in the WCR will be optically thin, with a spectral index of -0.1 . In combination with the stellar wind continuum from the binary system and Star C, this could result in a continuum spectrum that is flatter than a stellar wind spectrum if the thermal flux from the WCR is sufficiently high. The fluxes in the simulations of Pittard (2009) are two to three orders of magnitude less than observed in Cyg OB2 #5, attributable to the use of mass-loss rates \sim two orders of magnitude less than deduced here for Cyg OB2 #5. The optically-thin thermal flux scales as the

total number of ions in the WCR, which is $\propto \dot{M}^2/D$, where D is the distance from the binary to the WCR. Since the deduced mass-loss rate and separation in Cyg OB2 #5 are respectively ~ 100 and ~ 40 times those used in the simulations (cf. model cwb2 in Pittard 2009), the optically-thin flux from the WCR could be a similar order of magnitude as the observed fluxes. However, in this adiabatic scenario the flux variations scale as D^{-1} , and a highly eccentric orbit, as deduced in the $s = 0$ model presented above, spends the bulk of the orbit near apastron where D changes little. Hence, the flux would change little, contrary to the observations. Thus variable thermal emission from the WCR alone can not account for the radio light curves in Cyg OB2 #5, though free-free opacity through the circumbinary wind undoubtedly plays a role. This possibility needs to be explored further, though the types of models described by Pittard (2009) are beyond the scope of this paper.

Lastly, an alternative source of the X-ray and non-thermal radio emission could be a compact object such as a neutron star, though the estimated mass from the reflex motion analysis implies this possibility is remote. Though it is not clear how a compact object produces the radio emission, stellar wind accretion onto a $\sim 2 M_\odot$ compact star could generate the observed X-ray luminosity if gravitational potential can be converted to X-ray power efficiently. The gravitational capture radius of a neutron star of mass M_n for a stellar wind of velocity $v_\infty = 1500 \text{ km s}^{-1}$ is given by

$$R_g = \frac{2GM_n}{v_\infty^2} \sim 2.3 \times 10^{10} \text{ cm}.$$

Assuming the gravitational energy of the captured stellar wind is converted to X-ray emission with efficiency ϵ , then luminosity would be

$$L_x = \frac{GM_n \pi R_g^2 F_m(r) \epsilon}{R_n} \sim 3.1 \times 10^{41} F_m(r) \epsilon \text{ erg s}^{-1},$$

where $F_m(r)$ is the mass flux of stellar wind at distance r . For an orbit major axis of 14 AU and an eccentricity of 0.7 ($s = 0$ model), periastron separation is 4.2 AU at which distance $F_m = 4.3 \times 10^{-8} \text{ g cm}^{-2} \text{ s}^{-1}$ for a stellar wind mass-loss rate of $3.4 \times 10^{-5} M_\odot \text{ yr}^{-1}$. This gives $L_x \sim 3.4 L_\odot$ for $\epsilon = 1$, consistent with the $L_x = 1.5 L_\odot$ derived by Linder et al. (2009) and adjusted to a distance of 1.7 kpc .

4.3. The Secondary Source, NE

The spectral index of -0.50 ± 0.11 derived here indicates the radio emission from NE is non-thermal. This was previously suggested by Contreras et al. (1996) from a limit to the spectral index of -2.4 ± 0.6 deduced from one epoch of observations at 4.8 and 8.4 GHz in 1994 April. Contreras et al. (1997) were the first to note that NE lies directly between the Cyg OB2 #5 binary and a B-type star (Star D), $\sim 0.9''$ to the NE. This led them to propose that NE is the result of a WCR between the stellar wind of the Cyg OB2 #5 binary system with that from Star D. They further argued that the separation of NE from both the primary and Star D was consistent with the expected relative wind momenta of the binary and the B-type star. This assertion is re-examined here

based on seven epochs of 8.4-GHz observations of the primary and NE.

The position of the WCR relative to the positions of the sources of the colliding winds is given by

$$r_{\text{O+O}} = \left(1 - \frac{\eta^{1/2}}{1 + \eta^{1/2}}\right) D$$

(e.g. Eichler & Usov 1993) where D is the separation between the primary O-star binary (or triple) system and the B star, $r_{\text{O+O}}$ is the distance from the WCR to the primary system and η is the the wind-momentum ratio of the two stellar winds given by

$$\eta = \frac{\dot{M}_{\text{D}} v_{\text{D}}}{\dot{M}_{\text{O+O}} v_{\text{O+O}}}.$$

Here $\dot{M}_{\text{O+O}}$, \dot{M}_{D} , $v_{\text{O+O}}$ and v_{D} are the mass-loss rates and terminal-wind velocities of the O-star binary and Star D respectively. The separation of the O-star binary and the B-type companion is $D = 0.93 \pm 0.02''$ as determined from a weighted average of separations deduced from optical and IR observations (Sec. 2.4). Combined with $r_{\text{O+O}} = 0.77 \pm 0.08''$ measured here (Sec. 3.3), $\eta = 0.04^{+0.08}_{-0.03}$, where a Monte-Carlo method was used to determine the uncertainty in η as it is an ill-behaved function. Adopting $\dot{M}_{\text{O+O}} = 3.4 \times 10^{-5} M_{\odot} \text{ yr}^{-1}$ with $v_{\text{O+O}} = 1500 \text{ km s}^{-1}$ (Conti & Howarth 1999) leads to

$$\dot{M}_{\text{D}} = 0.5 - 6.1 \times 10^{-6} \left(\frac{1000 \text{ km s}^{-1}}{v_{\text{D}}}\right) M_{\odot} \text{ yr}^{-1}.$$

Keeping in mind the mass-loss rate of the binary is high compared with values deduced from model atmospheres, and the wind terminal speed for Star D is unknown, it is noted that only at the lower extremum is the mass-loss rate consistent with those expected for late-O/early-B supergiants, with early-B dwarfs having mass-loss rates around an order of magnitude lower (Mokiem et al. 2007), though it is noted that the IR photometry of Star D suggest a star that is more luminous than anticipated for a B0 dwarf. The need to consider the extremum mass-loss rate in order to account for the relative location of the binary, NE and Star D raises the question of whether NE is truly a WCR. However, the Wolf-Rayet system WR 147 provides a ready example of an early B-type dwarf star providing a sufficiently dense wind to give a readily observed WCR with the dense wind of a WN8 companion (Williams et al. 1997).

The proximity (in space) of Star D and the Cyg OB2 #5 binary can be tested by comparing their respective reddenings. Combining the K magnitude determined in Sec. 2.4 with the visual magnitude $V = 13.1 \pm 0.4$, derived by Contreras et al. (1997), gives $(V - K) = 5.5 \pm 0.4$ for Star D, assuming it does not vary. This implies a reddening of $A_V \simeq 6.9 \pm 0.5$ for Star D, greater than that ($A_V = 5.7 \pm 0.3$) implied by $(B - V) = 1.6 \pm 0.1$ measured by Contreras et al. (1997). In spite of this apparent discrepancy between visual and visual/IR-determined reddenings, the fact that the reddening estimates bracket that of Cyg OB2 #5 ($A_V = 6.4$), there is no reason to rule out an association between the binary and Star D, and hence the possibility that Cyg OB2 #5 is a quadruple system.

It is possible to estimate the luminosity of a WCR based upon the kinetic energy of the two colliding winds. The surface area of the WCR can be approximated as a spherical cap of diameter πr_{D} (Eichler & Usov 1993) where $r_{\text{D}} = D - r_{\text{O+O}}$ is the distance from Star D to the WCR. Using this area combined with the kinetic luminosity of the stellar wind of the binary, $L_{\text{O+O}} = 2.4 \times 10^{37} \text{ erg s}^{-1}$, leads to luminosity $L_{\text{WCR}} = 6.4 \times 10^{35} \text{ erg s}^{-1}$ entering the WCR. The radio synchrotron luminosity L_{syn} arising from the WCR, is estimated from $L_{\text{syn}} \sim 10^{-8} L_{\text{WCR}}$ (Chen & White 1994; Pittard & Dougherty 2006), giving an estimated synchrotron luminosity from the WCR of $\sim 6 \times 10^{27} \text{ erg s}^{-1}$. The radio luminosity of NE is estimated by integrating the observed continuum spectrum. Assuming a power-law spectrum between 0.1 - 100 GHz gives a synchrotron luminosity of $2.5 \times 10^{26} \text{ erg s}^{-1}$ for a distance of 1.7 kpc. Considering this is an order-of-magnitude argument, the synchrotron luminosity of the NE is closely consistent with that anticipated from a WCR.

An alternative model for NE is that of a background radio source in chance alignment with Cyg OB2 #5 and Star D. It is difficult to refute this possibility unequivocally, though the probability of such an alignment occurring randomly within 1 arcsecond of Cyg OB2 #5 is very low. Extragalactic source counts at 1.4 GHz indicate ~ 70 sources deg^{-2} of around 1 mJy (e.g. Jackson 2005), implying $\sim 10^{-6}$ of these sources in 1 arcsecond². If the source is at a much greater distance than Cyg OB2 #5 it will have a different proper motion to the binary. A distant galaxy will remain fixed relative to the reference frame of background quasars while the binary and Star D will exhibit proper motion relative to the frame. At radio wavelengths, it may be possible to measure this proper motion through astrometry. Certainly, the proper motion determined from the VLA observations discussed here is less than 100 mas, and to improve this precision would require VLBI observations. The low radio brightness of NE presents a challenge for higher precision VLBI astrometry. Alternatively, IR/optical imaging could reveal if NE is associated directly with an object. Cyg OB2 #5 is bright in the optical ($V=9.21$) and attempts at imaging the region between the binary system and Star D are thwarted by the high contrast of the binary and the large PSF of the imaging telescopes. The IR image (Sec. 2.4) was searched for evidence of a background source at the location of NE, but with no success. A smaller PSF could be attained by interferometry, but the contrast could only be defeated through either adaptive nulling or coronagraphic imaging. This observing challenge remains to be attempted.

5. SUMMARY

This paper re-examines over 50 VLA observations of the well-known O-star binary system Cyg OB2#5 in an attempt to locate and characterize the well-known variable radio emission in the system. The radio emission consists of a primary component that is associated with the binary system and a component to the NE. Both components are resolved in all 23 epochs of highest resolution VLA A-configuration observations, which reveal the flux of NE is constant while the flux of the primary varies. The constant flux from NE permits the flux of the primary to be derived in all observations for the first

time, most especially those where the two components are not resolved individually. A string-length analysis of the derived radio light curves of the primary emission at both 4.8 GHz and 8.4 GHz gives a period of 6.7 ± 0.3 years for the variations.

The primary emission changes character as it varies between its high state of ~ 8 mJy at 4.8 GHz and a spectral index of 0.24 ± 0.01 to a low emission state with a 4.8 GHz flux of ~ 2 mJy and a spectral index of 0.60 ± 0.04 , consistent with thermal emission from a stellar wind. Observations at 350 GHz obtained at an epoch not during a low emission state are also consistent with the thermal emission level observed during the low state, and hence lend support to the argument that the thermal emission observed during the low state remains relatively constant through the orbit.

The mass-loss rate of the binary is deduced to be $3.4 \times 10^{-5} M_{\odot} \text{ yr}^{-1}$ from the flux during the low emission state, which is unusually high for an Of supergiant, and comparable to the rates determined for WR stars. Together with the anomalous strength of the He I 1.083- μm emission line, also redolent of a WR star, this points to a fast, heavy wind and supports the suggestion by Bohannan & Conti (1976) that Cyg OB2 #5 is an immediate progenitor of a WR binary system in which the mass loss has not yet revealed enough evolved core material to affect the observed spectrum.

The flatter spectral index during the high state is attributed to the addition of a non-thermal component to the thermal emission from the binary stellar wind. A non-thermal source orbiting within the stellar wind envelope of the binary system every 6.7 years can account for the variations in radio flux through orbit modulation of the free-free opacity along lines of sight to the non-thermal source.

Such a model requires the presence of a third star in association with the binary system. The high luminosity of the binary components and the emission from the stellar wind make the detection of a third star challenging. An analysis of radial velocity data from the literature provides supporting evidence of reflex motion in the binary as a result of a third star, labelled Star C, with a mass of $23_{-14}^{+22} M_{\odot}$. Until further observations can be obtained, especially at orbital phases where the radial velocities change most dramatically, this provides a tantalizing piece of evidence that Cyg OB2 #5 is tertiary system rather than a binary. Additional support for a third star comes from a hard X-ray component, that Linder et al. (2009) suggest arises in a WCR between the binary wind and that of a third massive star.

This study also re-examines the NE source and its previous identification with a WCR between the winds of the O-star binary and that of a B0 star (Star D) $0.9''$ to the NE. Using MERLIN observations at 1.4 GHz

with the VLA observations confirms the non-thermal nature of NE with a spectral index of -0.50 ± 0.12 , and gives the relative separation of the binary and NE to be $0.77 \pm 0.08''$. Higher frequency radio observations would be useful to reveal the properties of the underlying relativistic electron population. Through wind-momentum balance, the mass-loss rate of Star D is estimated to be between $0.5 - 6.1 \times 10^{-6} M_{\odot} \text{ yr}^{-1}$, consistent with a late-O/early B supergiant at the lower extremum of this mass-loss rate range, and an order of magnitude too high for a lower luminosity star. This raises the possibility that NE is not a WCR, though the WR+B binary WR147 provides an example of an early B-type dwarf providing a sufficiently dense wind to give a readily observed WCR with the dense wind of a WN8 companion. Analysis of IR observations of Star D to the NE reveal an apparent discrepancy between visual and visual/IR-based reddening estimates, but provide no compelling reason to rule out an association between Cyg OB2 #5 and Star D, and hence the possibility that Cyg OB2 #5 is a quadruple system. An estimate of the non-thermal luminosity of NE is also consistent with a WCR. To test the alternative possibility that NE is an unassociated background source requires either high precision proper motion observations through VLBI, or deep optical IR imaging. Both of these possibilities require very challenging observations, that remain to be attempted.

The authors would like to thank Julian Pittard, Gregor Rauw, Mark Runacres, and Sven Van Loo for many useful discussions related to this work. This paper made extensive use of data from the National Radio Astronomy Observatory Very Large Array, New Mexico, USA, and the MERLIN array in England, UK. Thanks to Meri Stanley and the analysts team at NRAO and to Anita Richards at MERLIN for their help with the archive data. The National Radio Astronomy Observatory is a facility of the National Science Foundation operated under cooperative agreement by Associated Universities, Inc. MERLIN is a National Facility operated by the University of Manchester at Jodrell Bank Observatory on behalf of the Science and Technology Facilities Council (STFC) of the United Kingdom. The United Kingdom Infrared Telescope is operated by the Joint Astronomy Centre for the STFC. The James Clerk Maxwell Telescope is operated by The Joint Astronomy Centre on behalf of the STFC, the Netherlands Organisation for Scientific Research, and the National Research Council of Canada. The Carlos Sánchez Telescope (TCS) of the Observatorio del Teide (Tenerife) is operated by the Instituto Astrofísica de Canarias. Facilities: VLA, MERLIN, JCMT(Scuba), UKIRT(IRCAM3), TCS

REFERENCES

- Abbott, D. C., Biegging, J. H., & Churchwell, E. 1981, *ApJ*, 250, 645
 Biegging, J. H., Abbott, D. C., & Churchwell, E. B. 1989, *ApJ*, 340, 518
 Bohannan, B., & Conti, P. S. 1976, *ApJ*, 204, 797
 Chapman, J. M., Leitherer, C., Koribalski, B., Bouter, R., & Storey, M. 1999, *ApJ*, 518, 890
 Chen, W., & White, R. L. 1994, *Ap&SS*, 221, 259
 Conti, P. S., & Howarth, I. D. 1999, *MNRAS*, 302, 145
 Contreras, M. E., Rodriguez, L. F., Gomez, Y., & Velazquez, A. 1996, *ApJ*, 469, 329
 Contreras, M. E., Rodriguez, L. F., Tapia, M., Cardini, D., Emanuele, A., Badiali, M., & Persi, P. 1997, *ApJ*, 488, L153
 Crowther, P. A. 2007, *ARA&A*, 45, 177
 De Becker, M. 2007, *A&A Rev.*, 14, 171
 Dougherty, S., & Pittard, J. M. 2006, in *Proceedings of the 8th European VLBI Network Symposium*

- Dougherty, S. M., Pittard, J. M., Kasian, L., Coker, R. F., Williams, P. M., & Lloyd, H. M. 2003, *A&A*, 409, 217
- Ducati, J. R., Bevilacqua, C. M., Rembold, S. B., & Ribeiro, D. 2001, *ApJ*, 558, 309
- Dworetzky, M. M. 1983, *MNRAS*, 203, 917
- Eichler, D., & Usov, V. 1993, *ApJ*, 402, 271
- Fernie, J. D. 1989, *PASP*, 101, 225
- Fullerton, A. W., Massa, D. L., & Prinja, R. K. 2006, *ApJ*, 637, 1025
- Groh, J. H., Daminieli, A., & Jablonski, F. 2007, *A&A*, 465, 993
- Hall, D. S. 1974, *Acta Astronomica*, 24, 69
- Howarth, I. D., & Prinja, R. K. 1989, *ApJS*, 69, 527
- Jackson, C. 2005, *Publications of the Astronomical Society of Australia*, 22, 36
- Leung, K.-C., & Schneider, D. P. 1978, *ApJ*, 224, 565
- Linder, N., Rauw, G., Manfroid, J., Damerdji, Y., De Becker, M., Eenens, P., Royer, P., & Vreux, J.-M. 2009, *A&A*, 495, 231
- Miralles, M. P., Rodriguez, L. F., Tapia, M., Roth, M., Persi, P., Ferrari-Toniolo, M., & Curiel, S. 1994, *A&A*, 282, 547
- Mokiem, M. R., de Koter, A., Vink, J. S., Puls, J., Evans, C. J., Smartt, S. J., Crowther, P. A., Herrero, A., Langer, N., Lennon, D. J., Najarro, F., & Villariz, M. R. 2007, *A&A*, 473, 603
- Persi, P., Ferrari-Toniolo, M., & Grasdalen, G. L. 1983, *ApJ*, 269, 625
- Persi, P., Ferrari-Toniolo, M., Tapia, M., Rodriguez, L. F., & Roth, M. 1990, *A&A*, 240, 93
- Persi, P., Ferrari-Toniolo, M., Tapia, M., Roth, M., & Rodriguez, L. F. 1985, *A&A*, 142, 263
- Pittard, J. M. 2009, arXiv:0908.1003v2
- Pittard, J. M., & Dougherty, S. M. 2006, *MNRAS*, 372, 801
- Rauw, G., Vreux, J.-M., & Bohannan, B. 1999, *ApJ*, 517, 416
- Reid, R. I. 2006, *MNRAS*, 367, 1766
- Shepherd, M. C., Pearson, T. J., & Taylor, G. B. 1995, in *Bulletin of the American Astronomical Society*, ed. B. J. Butler & D. O. Muhleman, Vol. 27, 903
- Torres-Dodgen, A. V., Carroll, M., & Tapia, M. 1991, *MNRAS*, 249, 1
- Vacca, W. D., Garmany, C. D., & Shull, J. M. 1996, *ApJ*, 460, 914
- van Loo, S., Blomme, R., Dougherty, S. M., & Runacres, M. C. 2008, *A&A*, 483, 585
- Williams, P. M., Dougherty, S. M., Davis, R. J., van der Hucht, K. A., Bode, M. F., & Setia Gunawan, D. Y. A. 1997, *MNRAS*, 289, 10
- Williams, P. M., van der Hucht, K. A., Pollock, A. M. T., Florkowski, D. R., van der Woerd, H., & Wamsteker, W. M. 1990, *MNRAS*, 243, 662
- Wright, A. E., & Barlow, M. J. 1975, *MNRAS*, 170, 41